The effect of mass properties on road accident reconstruction

Massimilano Gobbi, Gianpiero Mastinu and Giorgio Previati*

Department of Mechanical Engineering, Politecnico di Milano, Milan, Italy

(*Received 19 February 2013; accepted 8 October 2013*)

1. Introduction

The reconstruction of road accidents is a very complex and delicate task. It is complex due to the complexity of the impact dynamics and lack of accurate data about the colliding vehicles. It is delicate due to the possible consequences (both economic and legal) of a non-accurate reconstruction. Road traffic has grown in the last few decades all over the world; consequently accidents between vehicles have grown as well. Worldwide, road accidents result in the death of more than 1.2 million people each year and between 20 and 50 million sustain non-fatal injuries [45]. In this scenario, the reconstruction of a car accident assumes a great importance in order to both prevent new crashes and ascribe responsibilities.

The aim when reconstructing an accident is to derive the initial position and velocities of all the vehicles involved in the crash. Two different approaches are currently employed for the estimation of such variables, one referring to the analysis of the data logged on the vehicles and the second by using a mathematical model able to simulate the motion of the vehicle before and after the crash [24]. The first approach requires vehicles equipped with data loggers such as Global Positioning System, tachographs and EDR (event data recorder) devices able to record the positions of the vehicle during the accident. These information can be used for the reconstruction; however, some uncertainties can arise from the measurement of the position and from the data analysis [4,24]. When such information are not available, only the second approach can be applied. By this approach, a mathematical model of the vehicles involved in the accident has to be used. Many mathematical models of colliding vehicles can be found in the literature [6,9,13,25,29,30,39,40,46]. The impact dynamics can be reconstructed by applying the basic principles of mechanics [13,25], on the basis of the data coming from the positions of the vehicles at rest and other data measured at the accident site and on the vehicles. Such models require a large number of parameters, referring to the vehicles and the environment, which can be only roughly estimated [3,38]. In particular, among others, the parameters that mostly affect the resulting motion of the vehicles are the pre-impact speed, the direction of travel, the position of the impact point [20,39], the crush coefficients [23,26,43], the coefficient of restitution [8,32,44] and the friction coefficient of the tyres on the road [2,16,41,42]. Usually a large number of simulations in which these parameters are varied are required to get the final position of the vehicle close to the one of the actual accident. Several papers can be found in the literature presenting automatic procedures able to change the values of the parameters and achieve a simulation complying with the actual measurements [10,22,34,35].

*Corresponding author. Email: giorgio.previati@polimi.it

In this paper, a procedure based on a quasi-random search followed by a simplex method is presented and validated against data recorded from actual accidents.

Different papers deal with the estimation of the uncertainties in the reconstruction of the accident given the uncertainty in the estimation of the parameters [5,7,12,17,18,21,33]. In most of these works the effect of the uncertainty in the knowledge of the mass properties (namely mass, centre of mass location and inertia tensor) of the colliding vehicles is not considered. However, in [18] the strong effects of such parameters are pointed out. In particular, the authors show that the moment of inertia around the vertical axis of the vehicle is responsible for large inaccuracies in the accident reconstruction, especially when post-impact rotations are involved. In the same research work, it is pointed out that among the considered parameters, only uncertainties on road friction have a stronger effect on accident reconstruction than the uncertainties on the mass properties (namely mass, centre of mass location and inertia tensor).

The second part of the present paper quantitatively assesses the effects of the errors in the estimation of the mass properties on the reconstructed accidents dynamics. In particular, the problem of the variation of the mass properties before and after the crash is discussed.

The paper is organised as follows. First, a description of the simulation model for accident reconstruction is presented. In addition, the identification procedure is presented along with an experimental validation of the method. Then, some real cases are considered in order to evaluate the effects of the errors of the mass properties on accidents reconstruction. Finally, a test rig able to measure the mass properties of a vehicle with the prescribed accuracy is presented [15].

2. Modelling the vehicle collision and the vehicle dynamics

The case of two colliding vehicles is considered. The mathematical model for this type of vehicle collision is described in Appendix 1. The vehicles are assumed to move on a flat horizontal plane. Their motions are described by, respectively, three degrees of freedom for each vehicle, namely, the yaw around a vertical axis and two displacements of the centre of gravity along the two coordinate axes (x and y, Figure 1). The impact is mathematically described (as introduced in [13] and in [25]) by referring respectively to the momentum and to the angular momentum conservation. The duration time of the impact is considered to be vanishing. The assumptions of plane motion and of three degrees of freedom are considered appropriate for modelling the collision of two vehicles as shown in [25]. The developed model is, therefore, applicable to all cases of frontal or lateral collision between two cars.

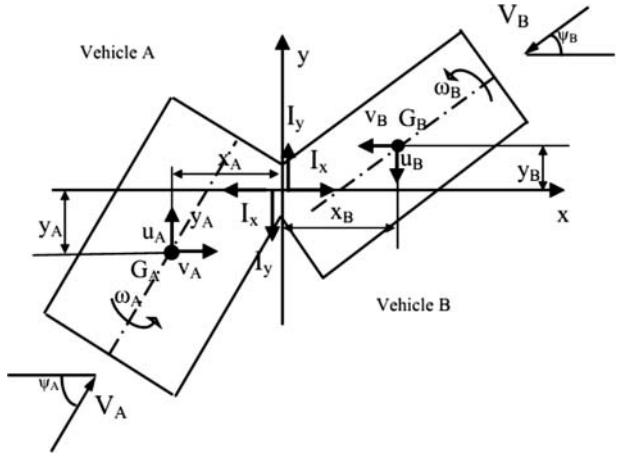

Figure 1. Oblique impact: general case.

The velocities of the two vehicles before the impact are given as initial guess data. By applying the momentum conservation and the angular momentum conservation, the velocities after the impact are computed. The motion after the impact of the two cars is computed by integrating nonlinear equations of motion of the vehicles. The initial conditions of the ordinary differential equations describing the motion of the vehicles come from the solution of the equations of momentum and of angular momentum conservation. The integration is performed by means of Simulink® (a MATLAB® tool). The forces acting on vehicles after the crash are calculated by considering a simplified tyre characteristic (the relationship between lateral force and lateral slip angle is bi-linear). The integration stops after a time pre-defined by the user or when the vehicle comes at rest.

Even if considering just the mechanical modelling of the dynamics and impact between two cars, the number of parameters needed to reconstruct the accident is very large. The complete list is reported in Appendices 2–4.

The energy dissipated, at each car, during the crushing process is estimated with the simple formula [25]

$$E_{\text{def}} = \frac{1}{2} K s^2, \tag{1}$$

where K is the crushing modulus and s is the final crush measured (mean value) on the deformed area of the car under consideration.

3. Implementation of the identification method

An accurate reconstruction of a road accident implies the introduction of correct data into the model described in the preceding section; such data are often unknown, so a proper identification procedure is needed. Referring to Table 1 and to the case studies presented in the subsequent sections, the actual implementation of an

Table 1. Flow chart of the procedure used to identify parameters in a road accident reconstruction.

Step	Action
1	Choosing the model (models) for describing the vehicle collision and the vehicle dynamics
2	Defining the parameters set that has to be identified
3	Defining the respective ranges (lower bound–upper bound) for the parameter values (feasible domain)
4	Defining a number n_c of parameter combinations whose values are uniformly distributed into the feasible domain (step #3) and performing the simulations
5	Sorting of the simulation results and refinement of the parameters sets by applying simplex minimisation algorithm

identification method for road accident reconstruction is presented below.

Step 1. The models for describing vehicle collisions and vehicle dynamics are those described in the previous section and in Appendix 1.

Step 2. The seven parameters (listed in Table 2) for the description of the collision and the six vehicle linear and angular speeds before the impact are defined as parameters to be identified. So (7 + 6) numerical values have to be defined, grouped into the vector $\overline{x}_p$.

Step 3. The parameter ranges $\overline{x}_{pmin} \leq \overline{x}_p \leq \overline{x}_{pmax}$ have to be set according to the experience of the user, usually with a variation of about 20% of the nominal values (see, e.g. Appendix 2). These ranges define the feasible domain of the parameters to be identified.

Step 4. The number n_c of parameter combinations (i.e. the number of vectors $\overline{x}_p$) whose values are uniformly distributed into the 13-dimensional feasible domain is defined by means of a proper mathematical theory (Sobol's uniformly distributed sequences) [28,31]. Such a theory allows obtaining uniformly distributed sequences over an n-dimensional domain. Among all of the available analytical sequences presented in [28,31], the LPτ distribution has proved to be more uniform and has been used here.

Therefore, for each of the n_c parameter combinations, the vehicle speed after the impact can be computed by applying the momentum conservation principle and the angular momentum conservation principle (see Appendix 1).

The variation of the total kinetic energy (ΔE_c) of the two vehicles before and after impact must be equal or slightly larger than the energy dissipated during the plastic deformation of the structures during the crushing process ($E_{\mathrm{def}A} + E_{\mathrm{def}B}$)

$$\Delta E_c = (E_{cA1} + E_{cB1}) - (E_{cA2} + E_{cB2}) \approx E_{\mathrm{def}A} + E_{\mathrm{def}B} \quad (2)$$

(as introduced in Appendix 1, the indexes A and B refer, respectively, to vehicles A and B, the indexes 1 and 2 refer to the instant before and after the impact).

The total energy dissipated at the impact is estimated in Equation (1) for each vehicle ($E_{\mathrm{def}A}$, $E_{\mathrm{def}B}$). The value of the dissipated energy for a vehicle should be bounded (neither too low, nor too high). The range is defined by the minimum and maximum crush modulus,

$$\begin{aligned} E_{\mathrm{def}A\mathrm{min}} &= \frac{1}{2}K_{A\mathrm{min}}s_A^2 \leq E_{\mathrm{def}A} \leq \frac{1}{2}K_{A\mathrm{max}}s_A^2 = E_{\mathrm{def}A\mathrm{max}} \\ E_{\mathrm{def}B\mathrm{min}} &= \frac{1}{2}K_{B\mathrm{min}}s_B^2 \leq E_{\mathrm{def}B} \leq \frac{1}{2}K_{B\mathrm{max}}s_B^2 = E_{\mathrm{def}B\mathrm{max}}. \end{aligned} \quad (3)$$

Table 2. Parameters and running conditions to be determined in the identification procedure.

#	Symbol	Parameter to be identified
1	α	Rotation angle of the (flat) impact surface with respect to a fixed reference system (°) (Figure 3)
2	e	Coefficient of restitution (–)
3	λ	Coefficient of interlocking and friction at the impact surface between two crushing vehicles (–)
4	K_A	Crushing modulus of vehicle A (–)
5	K_B	Crushing modulus of vehicle B (–)
6	f_A	Tyre–road friction coefficient – vehicle A (–)
7	f_B	Tyre–road friction coefficient – vehicle B (–)
#	Symbol	Running conditions to be defined (Figure 1)
8	V_{1A}	Velocity modulus before impact – vehicle A (m/s)
9	V_{1B}	Velocity modulus before impact – vehicle B (m/s)
10	θ_{1A}	Velocity direction before impact – vehicle A (°)
11	θ_{1B}	Velocity direction before impact – vehicle B (°)
12	Ω_{A1}	Vehicle A angular speed before impact (s^{-1})
13	Ω_{B1}	Vehicle B angular speed before impact (s^{-1})

K_A and K_B are not known precisely but they vary in predefined ranges depending on the actual vehicles involved in the accident. The crushes s_A, s_B are supposed to be measured.

If for a simulation case defined by a given parameter combination $\bar{x}_p$ the following equation holds:

$$\Delta E_c \approx E_{\mathrm{def}A} + E_{\mathrm{def}B} \tag{4}$$

then the simulation is considered to be 'physically consistent'. Typically the number n_{phc} of physically consistent cases is about one-half of the n_c considered cases. The data referring to physically consistent simulations are used to simulate the motion of the vehicles after the impact, until the rest positions are reached. The motion is simulated by integrating in the time domain the equations of motions of the two vehicles. The computed trajectories of the two vehicles refer to the 'impact point', defined as the centre of the 'impact surface' (the contact surface between the two crushing vehicles, whose centre is the origin O of the x–y axes in Figure 1).

For each one of the computed trajectories, the final rest position is considered. The error (ε) between the measured position at rest and the computed final position is determined referring to both the location of the centre of gravity (x, y) and the rotation of each vehicle (θ),

$$\begin{aligned} \varepsilon_{xA} &= x_{GA\mathrm{rm}} - x_{GA\mathrm{rc}} \quad & \varepsilon_{yA} &= y_{GA\mathrm{rm}} - y_{GA\mathrm{rc}} \\ \varepsilon_{\theta A} &= \theta_{GA\mathrm{rm}} - \theta_{GA\mathrm{rc}} \quad & \varepsilon_{xB} &= x_{GB\mathrm{rm}} - x_{GB\mathrm{rc}} \\ \varepsilon_{yB} &= y_{GB\mathrm{rm}} - y_{GB\mathrm{rc}} \quad & \varepsilon_{\theta B} &= \theta_{GB\mathrm{rm}} - \theta_{GB\mathrm{rc}}, \end{aligned} \tag{5}$$

where $x_{GA\mathrm{rm}}$ is the x coordinate of the centre of gravity of vehicle A at the measured rest position and $x_{GA\mathrm{rc}}$ is the x coordinate of the centre of gravity of vehicle A at the computed rest position. The meaning of other symbols can be inferred from the above explanation. The errors on centre of gravity location ($\varepsilon_{xA}, \varepsilon_{yA}, \varepsilon_{xB}, \varepsilon_{xB}$) and rotation ($\varepsilon_{\theta A}, \varepsilon_{\theta B}$) are returned together with the parameter vector $\bar{x}_p$ which describes each simulation.

Step 5. The vectors of errors defined in the previous step are sorted by using the well-known Pareto optimality theory [14,28]. Among the computed optimal set a limited number of solutions (up to 10) whose minimise the 'distance' with respect to the Utopia point are chosen as starting point ('initial guess') for the simplex minimisation algorithm. The simplex minimisation does not guarantee to reach a global minimum, so using different starting points for the final refinement of the sets of parameters, the probability to locate the global maximum is very high. For the minimisation by means of the simplex algorithm, a scalar normalised cost function is built as follows:

$$C = \frac{\sqrt{\varepsilon_{xA}^2 + \varepsilon_{yA}^2} + \sqrt{\varepsilon_{xB}^2 + \varepsilon_{yB}^2}}{E_{t\mathrm{adm}}} + \frac{|\varepsilon_{\theta A}| + |\varepsilon_{\theta B}|}{E_{\theta\mathrm{adm}}}. \tag{6}$$

$E_{\theta\mathrm{adm}}$ and $E_{\theta\mathrm{adm}}$ are the normalisation coefficients which have been defined on the basis of the admissible error thresholds that the operator can accept on the final location of the centre of gravity and on the rotation angle of the vehicle, respectively. The values have to be chosen on the basis of the user's experience.

4. Experimental validation

The proposed method for car accident reconstruction has been validated on the basis of real crash data found in the literature. For the considered accidents, the actual dynamics is known. In the following, three car accidents are considered. The three cases have been found in a report of the Japan Automotive Research Institute (JARI) published by Society of Automotive Engineers [10]. The principal parameters of the three cases, named JARI 1, JARI 4 and JARI 5, are summarised in Table 3 (detailed descriptions of the three cases are reported in Appendices 1–3).

4.1. *Case of study: JARI 1*

This case describes the oblique impact between two cars characterised by an angle of 46°. The impact, as reported in [10], is shown in Figure 2. The initial and final positions of the vehicles measured on a full-scale crash test are used to validate the methodology presented in this paper.

The vehicle parameters and the initial and final positions of the vehicles as reported in [10] are summarised in

Table 3. Principal parameters of the three considered accident cases JARI 1, JARI 4 and JARI 5 (details in Appendices 1–3, data from [10]).

Scenario Impact type		JARI 1 Oblique (46°)	JARI 4 Lateral (low speed)	JARI 5 Lateral (high speed)
Vehicle A	Mass (kg)	981	1737	977
	Initial velocity (m/s)	13.9	13.8	23.1
Vehicle B	Mass (kg)	974	1728	976
	Initial velocity (m/s)	13.8	11.8	22.8

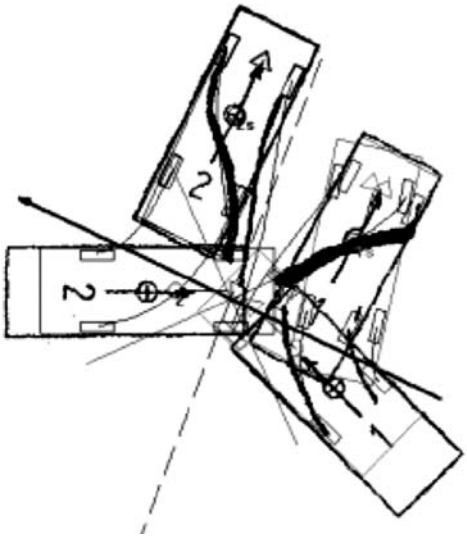

Figure 2. JARI 1 test case, adapted from [10].

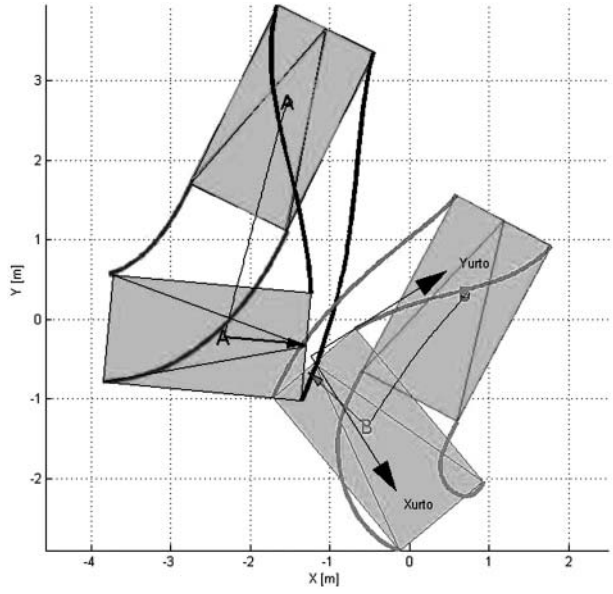

Figure 4. JARI 1 test case, best simulation solution.

Appendix 2. In Figures 3 and 4, two optimal solutions found by uniformly sampling the parameter space are shown. The two solutions show a good agreement with the final positions and rotations of the accident, even if some level of inaccuracy is present.

Figure 4 shows the final solution of the identification process (phase 5 in Table 1). As it can be seen, the position and rotation errors are negligible. The estimated initial velocities (before the impact) are 12.9 and 13.4 m/s (−6% and −3% with respect to the actual speed) for vehicles A and B, respectively. The estimated coefficient of restitution is 0.20 and the coefficient of interlocking and friction at the impact surface between two crushing vehicles is 0.57.

4.2. *Case of study: JARI 4*

This case study is of a lateral impact between two vehicles. After the impact, the two vehicles show some rotations around the yaw axis. In Figure 5, the scheme of the impact reported in [10] is shown. The data concerning this case are reported in Appendix 3.

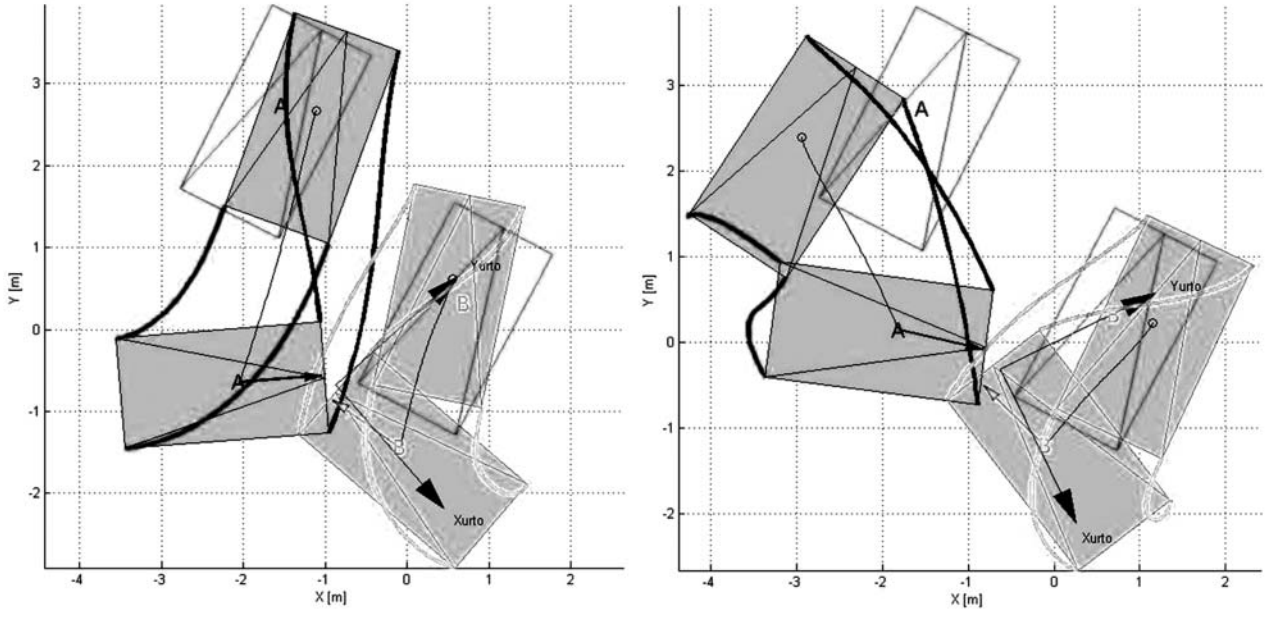

Figure 3. JARI 1 test case, two solutions at the end of phase 5 of Table 1. These solutions are used for further refinement (see Figure 4).

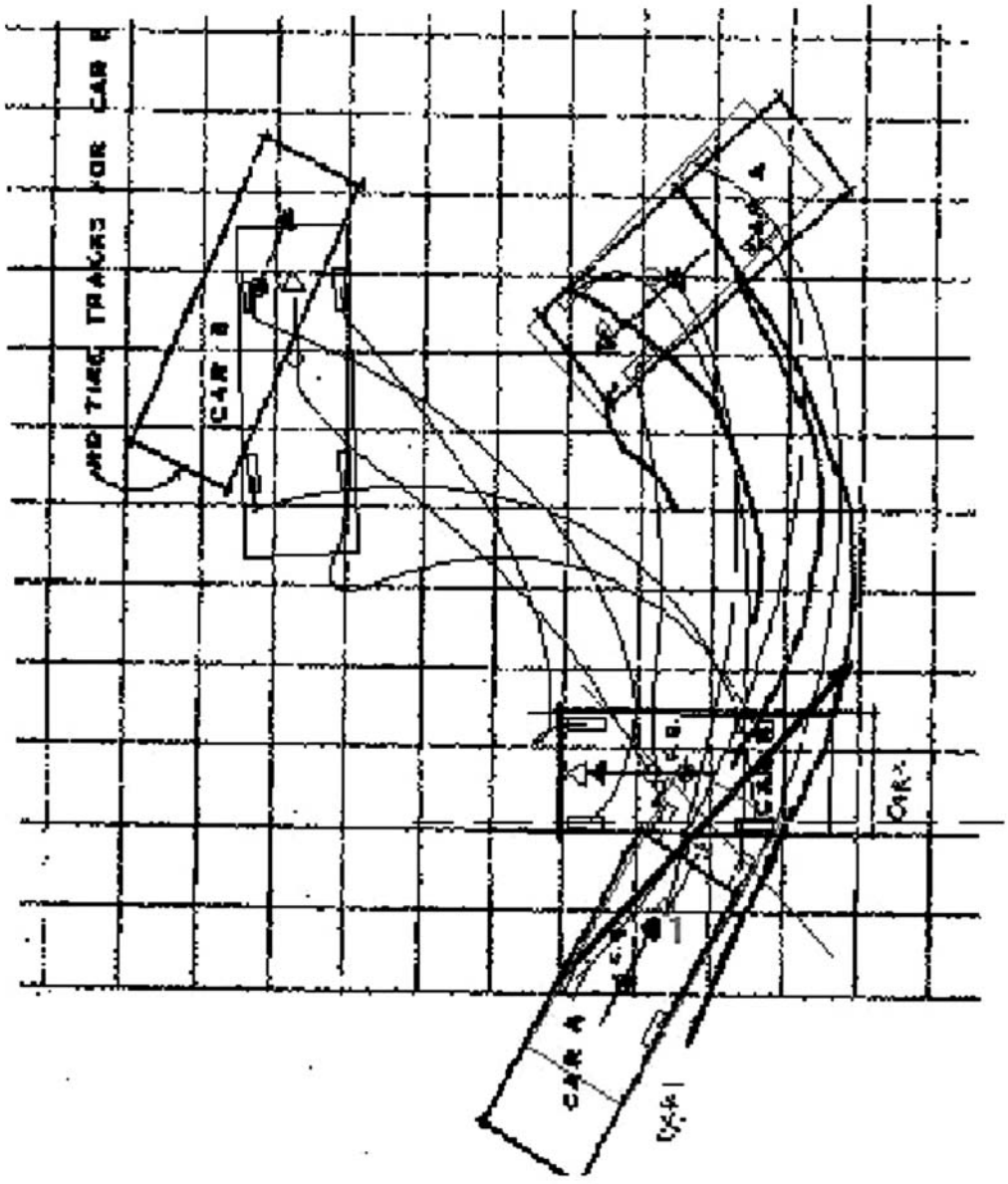

Figure 5. JARI 4 test case, adapted from [10].

Figure 6 shows the best simulation solution for the test case JARI 4 obtained by the reconstruction procedure described in the paper. Also for this scenario, the software is able to correctly identify the final location of the vehicles. However, the identification error of the initial speed of vehicle A is 12%, the one of vehicle B is 13%. It is not sure that better results could be obtained referring to a more refined model. Actually a refined model (with suspension system, tyre characteristics, etc.) would require more parameters. Increasing the number of uncertain parameters could add simulation errors compensating the more accuracy provided by the refined model.

4.3. Case of study: JARI 5

This case study is of a lateral impact between two vehicles at high speed. After the impact, the two vehicles show some rotations around the yaw axis and rest quite far from the collision point. In Figure 7 the scheme of the impact reported in [10] is shown, along with the proposed reconstruction. The data concerning this case are reported in Appendix 4.

Figure 8 shows the best simulation solution for the test case JARI 5 obtained by the reconstruction procedure described in the paper. On the left, the figure depicts the best solution after the sampling of the parameter domain

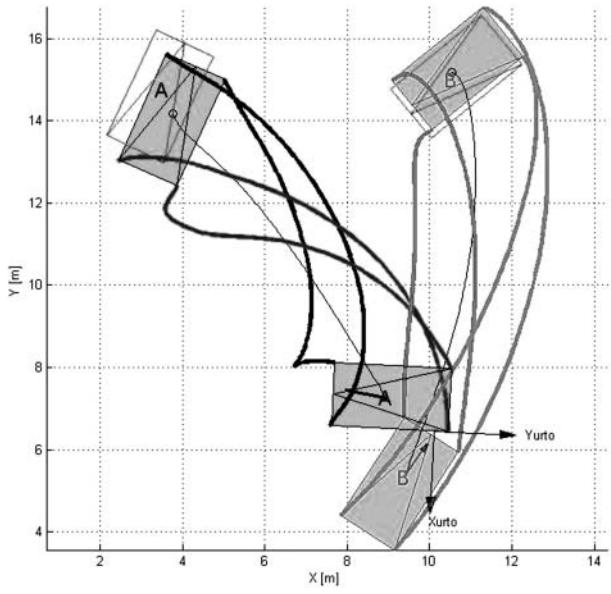

Figure 6. JARI 4 test case, best simulation solution.

(phase 4 of Table 2), while on the right the refined solution obtained by the simplex algorithm is reported (phase 5 of Table 2). The results show a very good capability of the procedure to reproduce the crash and post-impact dynamics of the vehicles, even in such a complex scenario. In fact, the high vehicle speeds and the large after-crash distances make the reconstruction of this scenario particularly difficult.

5. Effects of inaccuracy of the estimation of the mass properties on accidents reconstruction

The centre of gravity location and the value of the moments of inertia of a vehicle are very often roughly estimated even for uncrashed cars. The actual measurement of these parameters is quite complex and normally it is neglected. Moreover, the values of these parameters change as the vehicle is deformed during the impact, so the parameters estimated for the undeformed vehicle should not be used for the computation of the post-impact dynamics.

In this section the three different case studies, namely JARI 1, JARI 4 and JARI 5 [10], used for the validation of the presented reconstruction procedure are considered to assess the effects of errors in the estimation of both the location of the centre of gravity and the value of the yaw moment of inertia. First, the orders of magnitude of the typical variations in the centre of gravity location and in the value of the moment of inertia are estimated. Then, the effects of such variations on the reconstruction of the actual accident are evaluated.

5.1. Estimation of the change in the centre of gravity location and in the moment of inertia

For estimating the order of magnitude of the variation in the location of the centre of gravity and in the moment of inertia around the vertical axis of the vehicle, let us refer to Figure 9 where a frontal crash test of a mid-size vehicle is considered [19]. The impact is a frontal–lateral impact

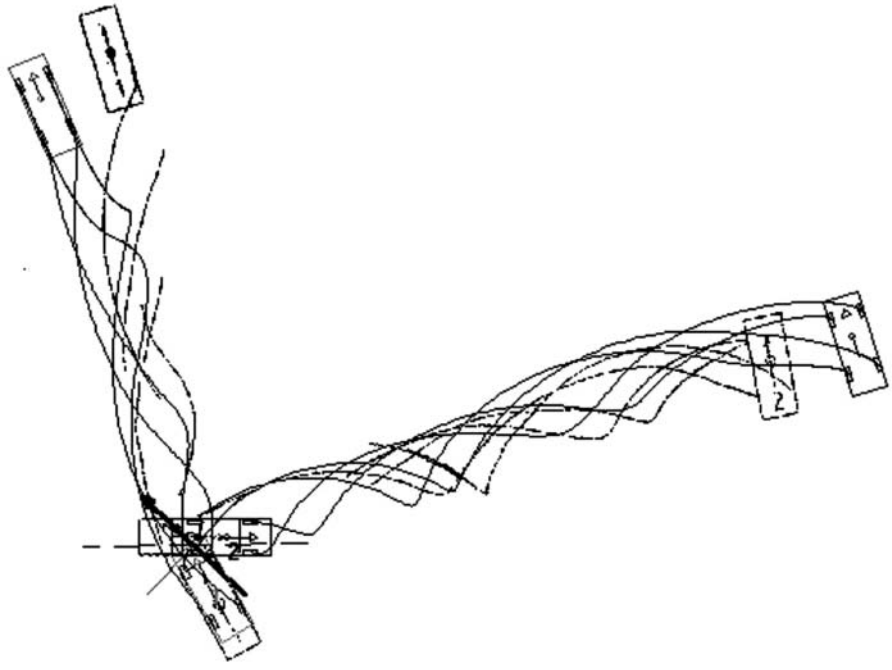

Figure 7. JARI 5 test case, adapted from [10].

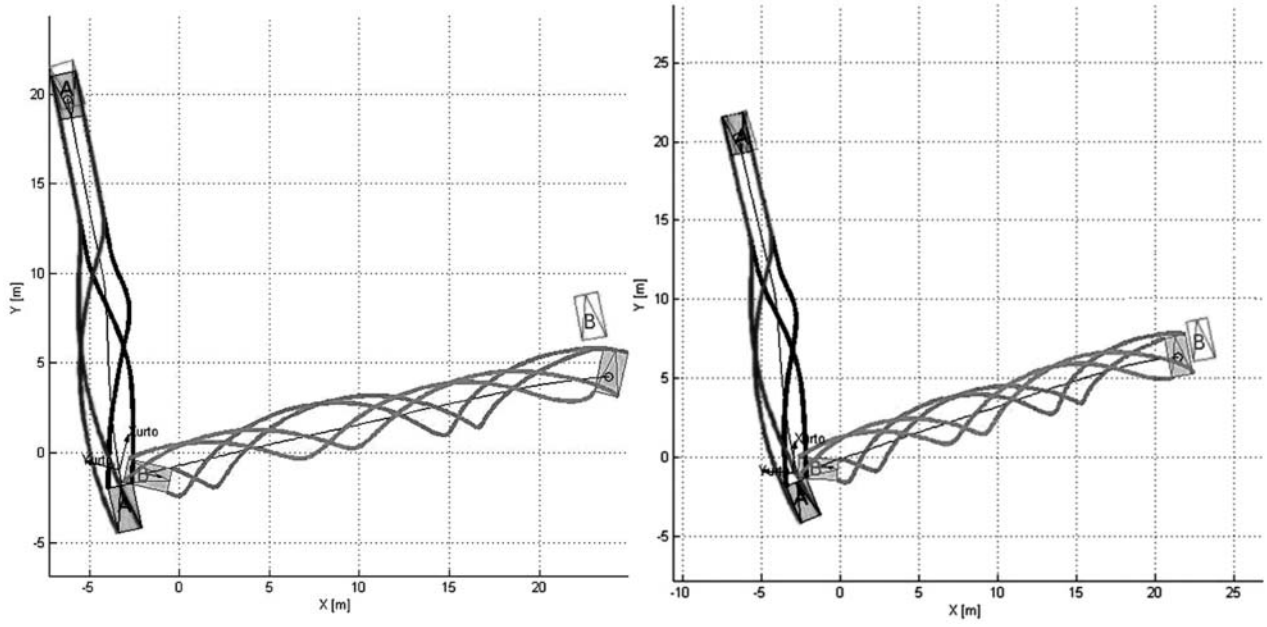

Figure 8. JARI 5 test case. Left: best simulation solution after phase 4 of Table 2. Right: best simulation solution after phase 5 of Table 2.

at 64 km/h. The vehicle shows a relevant deformation in its front part, while the rear part is almost undeformed. The reduction in the length of the vehicle can be estimated close to 500 mm.

In Figure 10, the vehicle before and after impact is shown. The total mass of the vehicle is 1550 kg. We consider a weight distribution of 55% at the front axle and a wheelbase of 2596 mm; the location of the centre of gravity of the vehicle (point C) is reported in Figure 10. Point A defines the location of the centre of gravity of the portion of the vehicle that will be deformed during the impact. The mass of this part is estimated as 500 kg. Point B refers to the location of the centre of gravity of the portion of the vehicle that will not be deformed during the impact (estimated mass of 1050 kg). If we consider a displacement of 300 mm of the centre of gravity of the part

Figure 9. Frontal crash test at 64 km/h, adapted from [19].

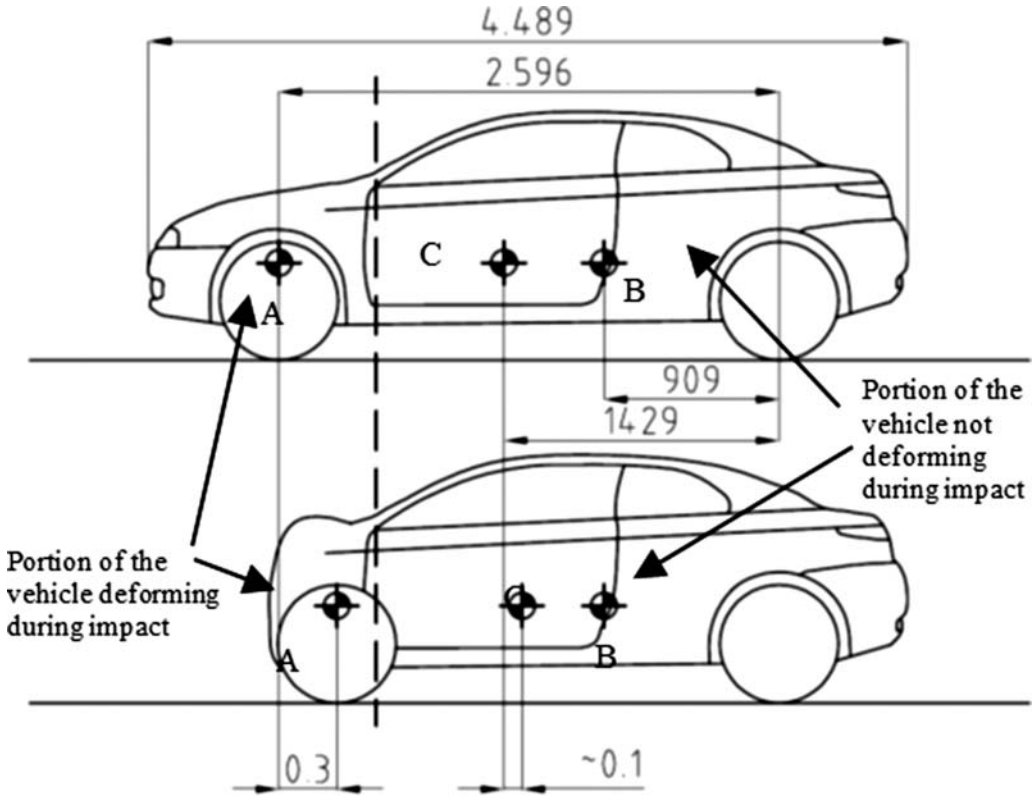

Figure 10. Estimation of the variation of centre of gravity location. A: centre of gravity of the portion of the vehicle deforming during impact. B: centre of gravity of the portion of the vehicle not deforming during impact. C: location of the centre of gravity of the vehicle.

of vehicle that will deform during the impact, the centre of gravity of the full vehicle will move backward around 100 mm due to the impact. These variations are typical for a crashed vehicle.

The value of the moment of inertia around the vertical axis of the vehicle can be roughly estimated by considering the vehicle as a parallelepiped with uniform mass [1],

$$k = \frac{1}{12} m(L^4 + W^4) \tag{7}$$

k being the moment of inertia, m being the mass, L being the length and W being the width. By considering an initial length of the vehicle of 4489 mm and a width of 1763 mm, the estimated moment of inertia of the vehicle (before crash) is 3000 kg m^2. If a reduction of 500 mm in length happens during the impact, the new moment of inertia is 2460 kg m^2 with a variation of 20%. A much more accurate way to obtain the moment of inertia of the vehicle before and after crash will be presented in Section 6.

Given the estimated variations in the location of the centre of gravity and in the moment of inertia after an impact, in the following, variations up to 150 mm in the coordinates of the centre of gravity and up to 50% in the moment of inertia will be considered.

5.2. *Variation of the position of the centre of gravity*

The location of the centre of gravity of one of the vehicles is varied according to the estimation given in the previous section, in a range ±150 mm in the longitudinal direction and ±150 mm in the lateral direction. For JARI 1 and JARI 4 the variation is on vehicle A, for JARI 5 on vehicle B. In Table 4 the effects of these variations on the global identification error (Equation (6)) are reported. Table 4 is constructed by integrating the motion of the vehicles, with different locations of the centre of gravity, with the same initial velocities and impact parameters found for the best simulation solutions found or the three scenarios. Figures 11–13 show the final position found for the two vehicles in the three scenarios for a displacement of +100 mm in the location of the centre of gravity of one of the vehicles in the longitudinal direction (best simulation solutions are reported in Figures 4, 6 and 8). The black rectangles in the figures represent the areas in which the differences in the final position of the two vehicles are considered ‘not relevant’. In other words if a car comes at the final static position fully inside the rectangle, the difference is not considered relevant.

It can be noticed that depending on the type of accident, significant errors in the final position of a vehicle are due even to the relatively limited variation of the centre of gravity in just one direction. Table 5 shows the effects of

Table 4. Effects of the variation of the centre of gravity (CG) location of one of the vehicles along the x axis (vehicle A for JARI 1 and JARI 4, vehicle B for JARI 5).

	Global position error (cost function of Equation (6)) normalised with respect to the error value when the reference CG position is considered		
Scenario	JARI 1	JARI 4	JARI 5
Reference CG location	1	1	1
+50 mm	17.0	3.7	1.5
+100 mm	41.5	9.2	2.1
+150 mm	74.6	16.9	3.9
−50 mm	27.4	4.0	1.8
−100 mm	67.1	6.9	3.0
−150 mm	121.5	9.8	4.8

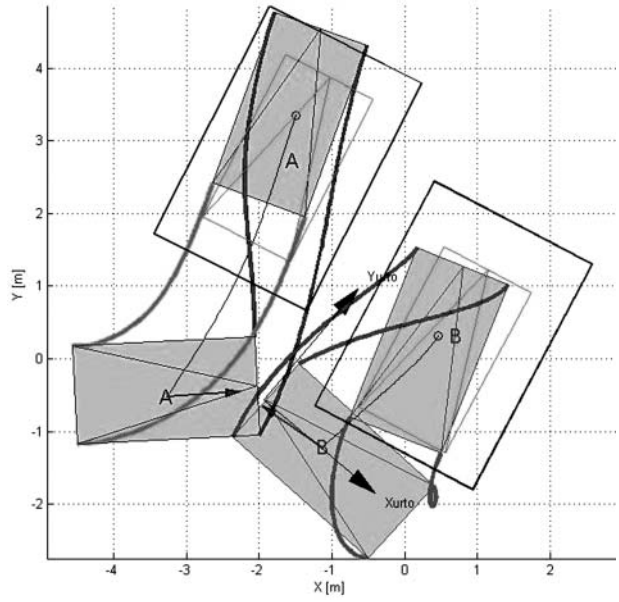

Figure 11. JARI 1 test case. Variation of 100 mm in the longitudinal direction of the centre of gravity location of vehicle A. Black rectangles represent the areas in which the differences in the final position of the two vehicles are considered not relevant.

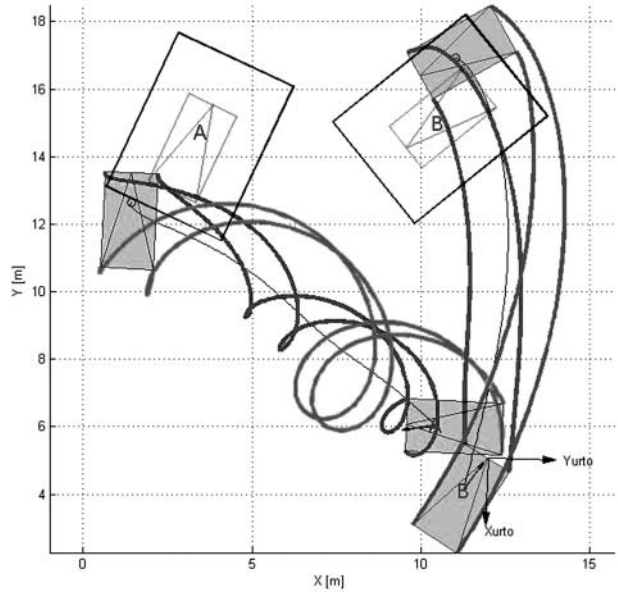

Figure 12. JARI 4 test case. Variation of 100 mm in the longitudinal direction of the centre of gravity location of vehicle A. Black rectangles represent the areas in which the differences in the final position of the two vehicles are considered not relevant.

lateral variation of the centre of gravity location for the three scenarios.

For the JARI 4 scenario, a sensitivity analysis on the identified initial velocities for a variation of the centre of gravity location has been performed. Table 6 reports the initial velocities found for a variation of 100 mm in the longitudinal and lateral positions of the centre of gravity of vehicle A. The table is built by applying the identification procedure considering the new locations of the centre of gravity of vehicle A. By inspecting Table 6, it can be noticed that the location of the centre of gravity has a huge influence on both the translational and rotational velocities. The variation in the translational velocities is up to 25%, while the rotational velocities, in some other examined cases, have been found to change their sign!

5.3. *Variation of the yaw moment of inertia*

The same procedure of the previous section has been applied to a variation of the value of the yaw moment of inertia in the range ±50% (see Section 5.1). For JARI 1 and JARI 4 the variation is on vehicle A, for JARI 5 on vehicle B (results shown in Figures 14–16). In Table 7, the effect of this variation in the computed global error is shown, while in Table 8 the effect of an increment of 10% of this parameter on the identified initial velocities is reported.

Table 8 shows that even a relative small error of 10% on the estimated value of the moment of inertia can lead to an error of close to 20% on the translational velocities and to the change of the sign of the rotational velocities.

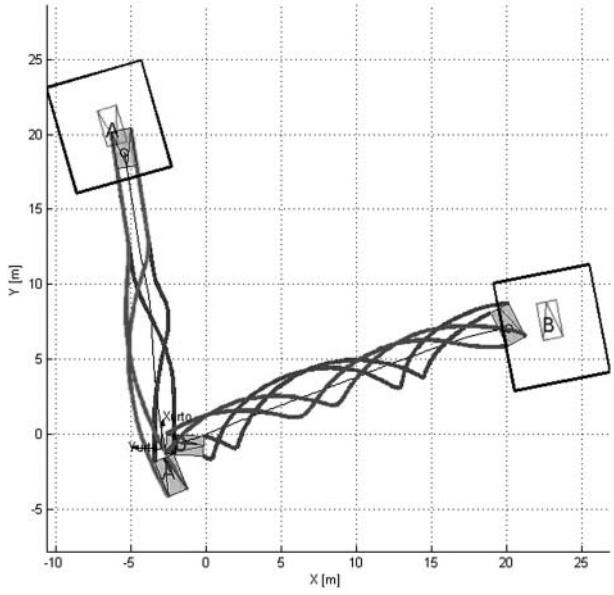

Figure 13. JARI 5 test case. Variation of 100 mm in the longitudinal direction of the centre of gravity location of vehicle A. Black rectangles represent the areas in which the differences in the final position of the two vehicles are considered not relevant.

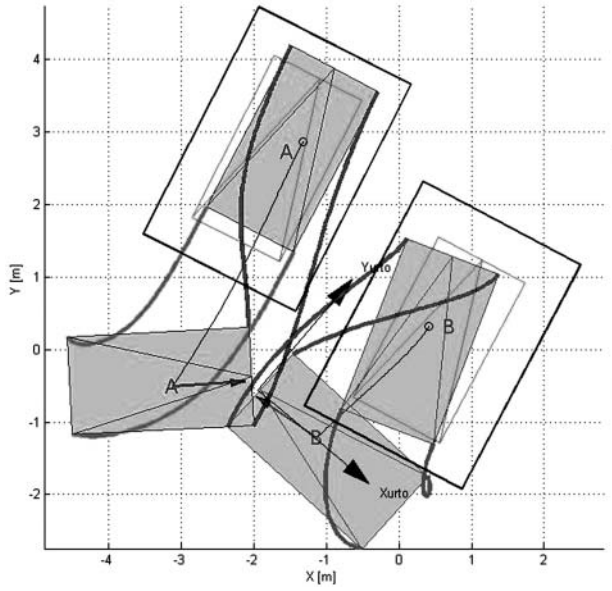

Figure 14. JARI 1 test case. Variation of −30% of the moment of inertia along the vertical axis of vehicle A. Black rectangles represent the areas in which the differences in the final position of the two vehicles are considered not relevant.

For larger error in the estimated values of the yaw moment of inertia completely erratic reconstructions of the accident can be obtained, as it is shown in Figure 15.

Summarising, even relatively small errors (50 mm) on the location of the centre of gravity or on the yaw moment of inertia (10%) can lead to inaccurate, if not erratic, reconstructions of the initial conditions of the motion of the vehicles involved in the accidents. As the initial velocities increase or when the after-crash trajectories are complex, higher accuracy on the knowledge of these parameters is required.

In the next section, a test rig able to measure the inertia properties for crashed and uncrashed vehicles with an accuracy well within the stated ranges will be presented.

Table 5. Effects of the variation of the centre of gravity location of one of the vehicles along the y axis (vehicle A for JARI 1 and JARI 4, vehicle B for JARI 5).

	Global position error (cost function of Equation (6)) normalised with respect to the error value when the reference CG position is considered		
Scenario	JARI 1	JARI 4	JARI 5
Reference CG location	1	1	1
+50 mm	31.4	3.8	1.9
+100 mm	94.9	9.6	4.3
−50 mm	45.6	3.1	2.1
−100 mm	149.7	8.3	7.2

Table 6. Effect of 100 mm of displacement of the centre of gravity of vehicle A on the identified initial velocities. Considered scenario: JARI 4.

		+100 mm CG (longitudinal)		−100 mm CG (lateral)	
	Reference	Value	% error	Value	% error
V_{1A} (m/s)	13.6	11.8	13.2	10.2	25.0
ω_{1A} (s^{-1})	−0.42	−0.67	−59.5	−0.78	−85.7
V_{1B} (m/s)	19.6	15.8	19.4	17.5	10.7
ω_{1B} (s^{-1})	−0.18	0.43	338.9	0.74	511.1

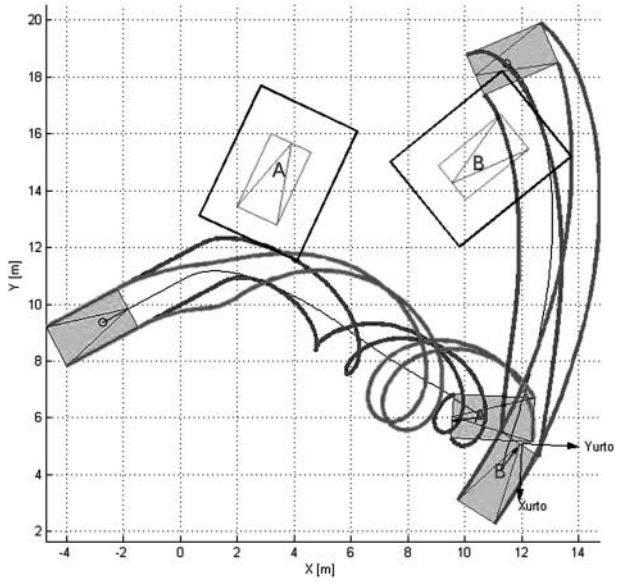

Figure 15. JARI 4 test case. Variation of −30% of the moment of inertia along the vertical axis of vehicle A. Black rectangles represent the areas in which the differences in the final position of the two vehicles are considered not relevant.

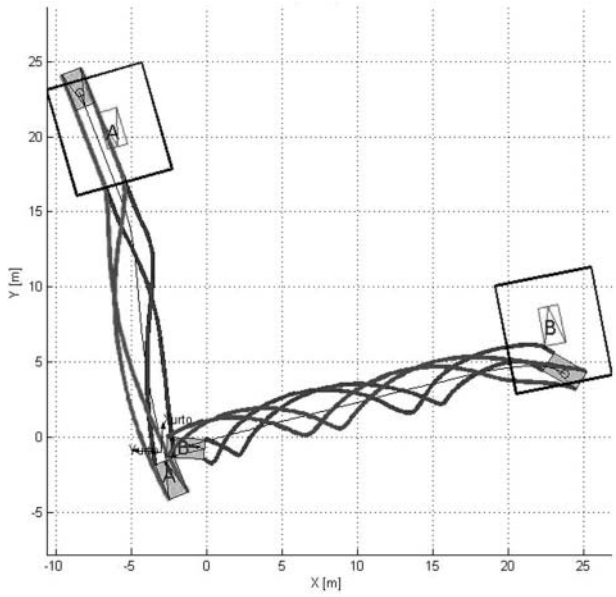

Figure 16. JARI 5 test case. Top: best simulation solution. Bottom: variation of −30% of the moment of inertia along the vertical axis of vehicle A. Black rectangles represent the areas in which the differences in the final position of the two vehicles are considered not relevant.

5.4. Effect of the payload

The effect of the passenger and payload on the inertia properties of the vehicle plays for sure a role in the reconstruction of the accident. This effect is strongly variable with the location of the payload, with the type of vehicle involved in the accident and may deserve a dedicated work. Anyway, the focus of the analysis presented in this paper is the estimation of the effects of errors on the estimation of the mass properties of the vehicle on the accident reconstruction, regardless if the errors are due to the payload or due to the vehicle itself.

6. Test rig for the measurement of the inertia properties of crashed and uncrashed vehicles

A method for the accurate measurement of the centre of gravity location and of the inertia tensor of full-scale vehicles is presented. The proposed method has been developed at the Politecnico di Milano (Technical University of Milan) and is called InTenso+ test system. The test rig is a device for the identification of the inertia tensor of rigid bodies [11,15,27,36,37] and it is basically a multicables pendulum carrying the body under investigation. The pendulum is swung from well-defined initial conditions, its motion is recorded by means of encoders and the loads acting on the cables are measured; the full inertia tensor is derived by means of a proper mathematical procedure.

In Figure 17, the test rigs are shown while measuring the inertia properties of a car. The test rig is composed of a frame for carrying a rigid body and four (or three) cables connecting this frame to another external frame fixed near the ceiling of the laboratory. The specifications of the test

Table 7. Effects of the variation of the yaw moment of inertia of one of the vehicles (vehicle A for JARI 1 and JARI 4, vehicle B for JARI 5).

	Global position error (cost function of Equation (6)) normalised with respect to the error value when the reference yaw moment of inertia is considered		
Scenario	JARI 1	JARI 4	JARI 5
Reference yaw moment of inertia	1	1	1
+10%	10.4	5.0	1.6
+30%	29.0	11.9	3.7
+50%	45.8	17.4	8.1
−10%	15.5	5.2	1.6
−30%	55.4	43.3	18.3
−50%	186.9	178.9	50.6

Table 8. Effect of 10% variation of the yaw moment of inertia of vehicle A on the identified initial velocities. Considered scenario: JARI 4.

		+10% moment of inertia	
	Reference	Value	% error
V_{1A} (m/s)	13.6	11.3	16.9
ω_{1A} (s^{-1})	−0.42	−0.80	−90.5
V_{1B} (m/s)	19.6	18.3	6.6
ω_{1B} (s^{-1})	−0.18	0.72	500.0

rig are reported in Table 9. The test rig is able to identify the mass properties with the accuracy needed for an accurate accident reconstruction: a few millimetres in the location of the centre of gravity and less than 1% in the yaw moment of inertia. Obviously, the test rig can be used for the measurement of crashed vehicles.

The test rig in Figure 17 can measure very quickly both the centre of gravity location and the inertia tensor of a crashed car. It possesses the ability to measure as accurately as needed the inertia parameters that are imperative for performing accurate accident reconstructions (test rigs specifications in Table 8).

7. Conclusion

In this paper a mathematical procedure for the reconstruction of road accidents has been presented and used to assess the influence of vehicle mass properties (namely location of the centre of gravity and yaw moment of

Table 9. InTenso+ and InTensino+ test rigs specifications.

Test rig	InTenso+
Payload range (kg)	500–3500
Maximum dimensions of the body ($L \times W \times H$) (mm)	$7000 \times 2000 \times 1600$[a]
Motion frequency (Hz)	<5
Peak acceleration during test (min–max) (m/s^2)	2–10
CG uncertainty (in plane, height) (mm)	±3–±5
Moment of inertia (MOI) uncertainty	±1%
Product of inertia (POI) accuracy (% of the maximum MOI of the body)	±0.5%
MOI and POI resolution (% of the maximum MOI of the body)	0.2%
Testing time (min)[b]	<10

[a]Dimensions are indicative. Fully customised fixturing can be realised.
[b]The testing time does not consider the time needed to position the body on the test rig.

Figure 17. InTenso+ test rig.

inertia). If the final locations of the two crashed cars are known, the mathematical procedure can be used to identify the vehicle speeds before the impact. Together with the speeds, the most important parameters influencing the motion of the vehicle during and after the impact are identified (tyre–road friction, crush parameters, etc.).

Some real cases presented in the literature have been considered to validate the procedure. The procedure has proved to be able to identify accurately both the final location of the vehicles and the respective speeds of the vehicles before impact.

A sensitivity analysis has been performed in order to evaluate the influence on accident reconstruction accuracy of the centre of gravity location and of the moment of inertia of vehicles. Such parameters have a relevant effect on the computed dynamics. Without an accurate measurement of these parameters, errors of the order of 20%–25% can be found in the translational velocities of the vehicles, while the rotational velocity can be completely wrong (even the rotation direction can switch).

A variation of 100 mm in the longitudinal or lateral position of the centre of gravity of one vehicle has a very large influence on both the estimated initial translational and rotational velocities which can lead to a completely wrong reconstruction.

Similar levels of errors can be obtained with a variation of 10% on the value of the yaw moment of inertia. For larger variations in the estimated values of the yaw moment of inertia, completely erratic reconstructions can be obtained.

A test rig (InTenso+) able to measure the centre of gravity location and the inertia tensor with the required accuracy has been introduced and briefly described in the paper.

References

[1] R.W. Allen, T.J. Rosenthal, and H.T. Szostak, *Steady state and transient analysis of ground vehicle handling*, SAE Paper 870495, SAE International, Warrendale, PA, 1987.

[2] W. Bartlett and W. Wright, *Braking on dry pavement and gravel with and without ABS*, SAE Tech. Paper 2010-01-0066, SAE International, Warrendale, PA, 2010. doi:10.4271/2010-01-0066.

[3] W. Bartlett, W. Wright, O. Masory, R. Brach, A. Baxter, B. Schmidt, F. Navin, and T. Stanard, *Evaluating the uncertainty in various measurement tasks common to accident reconstruction*, SAE Tech. Paper 2002-01-0546, SAE International, Warrendale, PA, 2002. doi:10.4271/2002-01-0546.

[4] R. Bortolin, J. Hrycay, and J. Golden, *GPS device comparison for accident reconstruction*, SAE Tech. Paper 2012-01-0997, SAE International, Warrendale, PA, 2012. doi: 10.4271/2012-01-0997.

[5] R. Brach, *Uncertainty in accident reconstruction calculations*, SAE Tech. Paper 940722, SAE International, Warrendale, PA, 1994. doi:10.4271/940722.

[6] R. Brach and R. Brach, *Crush energy and planar impact mechanics for accident reconstruction*, SAE Tech. Paper 980025, SAE International, Warrendale, PA, 1998. doi:10.4271/980025.

[7] R. Brach, R. Brach, and A. Louderback, *Uncertainty of CRASH3 ΔV and energy loss for frontal collisions*, SAE Tech. Paper 2012-01-0608, SAE International, Warrendale, PA, 2012. doi:10.4271/2012-01-0608.

[8] P. Burkhard, *ΔV, BEV and coefficient of restitution relationships as applied to the interpretation of vehicle crash test data*, SAE Tech. Paper 2001-01-0499, SAE International, Warrendale, PA, 2001. doi:10.4271/2001-01-0499.

[9] W. Cliff and D. Montgomery, *Validation of PC-Crash – a momentum-based accident reconstruction program*, SAE Tech. Paper 960885, SAE International, Warrendale, PA, 1996. doi:10.4271/960885.

[10] W.E. Cliff and A. Moser, *Reconstruction of twenty staged collisions with PC-Crash's optimizer*, SAE Paper 2001-01-0507, SAE International, Warrendale, PA, 2001.

[11] C. Doniselli, M. Gobbi, and G. Mastinu, *Measuring the inertia tensor of vehicles,* 17th IAVSD Symposium, The Dynamics of Vehicles on Road and Tracks, Copenhagen, Denmark, 2001.

[12] G. Fleck and J. Daily, *Sensitivity of Monte Carlo modeling in crash reconstruction*, SAE Int. J. Passeng. Cars – Mech. Syst. 3 (2010), pp. 100–112. doi:10.4271/2010-01-0071.

[13] G. Genta, *Motor Vehicle Dynamics: Modeling and Simulation*, 2nd ed., World Scientific, London, UK, 2003.

[14] M. Gobbi, *A k, k-ε optimality selection based multi objective genetic algorithm with applications to vehicle engineering*, Optim. Eng. 14 (2) (2013), pp. 345–360.

[15] M. Gobbi, G. Mastinu, and G. Previati, *A method for measuring the inertia properties of rigid bodies*, Mech. Syst. Signal Process. 25 (2011), pp. 305–318. doi:10.1016/j.ymssp.2010.09.004.

[16] D.W. Goudie, J.J. Bowler, C.A. Brown, B.E. Heinrichs, and G.P. Siegmund, *Tire friction during locked wheel braking*, SAE Tech. Paper 2000-01-1314, SAE International, Warrendale, PA, 2000. doi:10.4271/2000-01-1314.

[17] F. Guan, A. Belwadi, and X. Han, *Application of optimization methodology on vehicular crash reconstruction*, Paper no. IMECE2009-12810, ASME International Mechanical Engineering Congress and Exposition (IMECE2009), Lake Buena Vista, FL, 2009, pp. 567–573.

[18] B. Heinrichs, B. Mac Giolla Ri, and R. Hunter, *Sensitivity of collision simulation results to initial assumptions*, SAE Int. J. Passeng. Cars – Mech. Syst. 5 (2012), pp. 807–832. doi:10.4271/2012-01-0604.

[19] http://www.euroncap.com/home.aspx, 2012.

[20] H. Ishikawa, *Impact center and restitution coefficients for accident reconstruction*, SAE Tech. Paper 940564, SAE International, Warrendale, PA, 1994. doi:10.4271/940564.

[21] A.M. Knox, *Multivariable Monte Carlo analysis methods in traffic accident reconstruction using Python*, Paper no. IMECE2011-62242, ASME International Mechanical Engineering Congress and Exposition (IMECE2011), Denver, CO, 2011, pp. 639–653.

[22] G. Kost and S. Werner, *Use of Monte Carlo simulation techniques in accident reconstruction*, SAE Tech. Paper 940719, SAE International, Warrendale, PA, 1994. doi:10.4271/940719.

[23] J. Lawrence, R. Fix, A. Ho, D. King, and P. D'Addario, *Front and rear car crush coefficients for energy calculations*, SAE Tech. Paper 2010-01-0069, SAE International, Warrendale, PA, 2010. doi:10.4271/2010-01-0069.

[24] Z. Lozia and M. Guzek, *Uncertainty study of road accident reconstruction – computational methods*, SAE Tech. Paper 2005-01-1195, SAE International, Warrendale, PA, 2005. doi: 10.4271/2005-01-1195.

[25] R.H. Macmillan, *Dynamics of Vehicle Collisions*, Interscience Enterprises, St. Helier, UK, 1989.

[26] M. Marine, J. Wirth, and T. Thomas, *Crush energy considerations in override/underride impacts*, SAE Tech. Paper 2002-01-0556, SAE International, Warrendale, PA, 2002. doi:10.4271/2002-01-0556.

[27] G. Mastinu, M. Gobbi, and C. Doniselli, *Device for measuring the inertia tensor of rigid bodies*, US. Patent no. US 7278295, 2003.

[28] G. Mastinu, M. Gobbi, and C. Miano, *Optimal Design of Complex Mechanical Systems with Applications to Vehicle Engineering*, Springer-Verlag, Berlin, 2006.

[29] G. Mastinu, M. Gobbi, and M. Mimini, *A parameter identification method for road accidents reconstruction*, Proceedings of IMECE ASME International Mechanical Engineering Congress (IMECE 2003-43016), Washington, DC, 2003.

[30] G. Mastinu, M. Gobbi, and G. Previati, *Influence of vehicle inertia tensor and centre of gravity location on road accident reconstruction*, Proceedings of the International Design Engineering Technical Conferences, Washington, DC, 2011.

[31] J.B. Matusov, *Multicriteria Optimisation and Engineering*, Chapman & Hall, New York, 1995.

[32] R. McHenry and B. McHenry, *Effects of restitution in the application of crush coefficients*, SAE Tech. Paper 970960, SAE International, Warrendale, PA, 1997. doi:10.4271/970960.

[33] L. Metz and L. Metz, *Sensitivity of accident reconstruction calculations*, SAE Tech. Paper 980375, SAE International, Warrendale, PA, 1998. doi:10.4271/980375.

[34] A. Moser and H. Steffan, *Automatic optimization of pre-impact parameters using post impact trajectories and rest positions*, SAE Tech. Paper 980373, SAE International, Warrendale, PA, 1998. doi:10.4271/980373.

[35] A. Moser, H. Steffan, A. Spek, and W. Makkinga, *Application of the Monte Carlo methods for stability analysis within the accident reconstruction software PC-CRASH*, SAE Tech. Paper 2003-01-0488, SAE International, Warrendale, PA, 2003. doi:10.4271/2003-01-0488.

[36] G. Previati, M. Gobbi, and G. Mastinu, *Method for the measurement of the inertia properties of bodies with aerofoils*, J. Aircraft 49 (2012), pp. 444–452.

[37] G. Previati, G. Mastinu, and M. Gobbi, *Advances on inertia tensor and centre of gravity measurement*, SAWE Paper no. 3465, Society of Allied Weight Engineers, Inc., Los Angeles, CA, 2008.

[38] B. Randles, B. Jones, J. Welcher, T. Szabo, D. Elliot, and C. MacAdams, *The accuracy of photogrammetry vs. hands-on measurement techniques used in accident reconstruction*, SAE Tech. Paper 2010-01-0065, SAE International, Warrendale, PA, 2010. doi:10.4271/2010-01-0065.

[39] H. Steffan, *Accident reconstruction methods*, Vehicle Syst. Dyn. 47 (2009), pp. 1049–1073.

[40] H. Steffan and A. Moser, *The collision and trajectory models of PC-CRASH*, SAE Paper 96-0886, SAE International, Warrendale, PA, 1996.

[41] D. Vangi and A. Virga, *Evaluation of emergency braking deceleration for accident reconstruction*, Vehicle Syst. Dyn. 45 (2007), pp. 895–910.

[42] M.S. Varat, J.F. Kerkhoff, S.E Husher, C.D. Armstrongand, and K.F. Shuman, *The analysis and determination of tire-roadway frictional drag*, SAE Tech. Paper 2003-01-0887, SAE International, Warrendale, PA, 2003. doi:10.4271/2003-01-0887.

[43] K. Welsh and D. Struble, *Crush energy and structural characterization*, SAE Tech. Paper 1999-01-0099, SAE International, Warrendale, PA, 1999. doi:10.4271/1999-01-0099.

[44] D. Wood, *Structural rebound characteristics of the car population in frontal impacts*, SAE Tech. Paper 2000-01-0461, SAE International, Warrendale, PA, 2000. doi:10.4271/2000-01-0461.

[45] World Health Organization, *Global Status Report on Road Safety: Time for Action*, WHO Press, Geneva, 2009.

[46] J. Zebala, W. Wach, P. Ciepka, R. Janczur, and S. Walczak, *Verification of ABS models applied in programs for road accident simulation*, SAE Int. J. Passeng. Cars – Mech. Syst. 3 (2010), pp. 72–99. doi:10.4271/2010-01-0070.

Appendix 1. Simplified dynamics of vehicle collision

In this appendix, the theory presented in [25] and (with some amendments) in [13] is summarised.

Given two isolated bodies crushing one against the other, all contact and aerodynamic forces can be considered vanishing during the impact and only the impact forces remain. The system can be considered as isolated and the moment conservation equation can be written as

$$m_A v_{A_1} + m_B v_{B_1} = m_A v_{A_2} + m_B v_{B_2}, \tag{A1}$$

where m_A and m_B refer to the mass of vehicles A and B, respectively, and the other symbols refer to Figure 1. Subscript 1 refers to an instant before the impact and subscript 2 refers to an instant after the impact.

The conservation principle is valid for total energy, while the kinetic energy is partly converted into deformation energy and other kinds of energy, so that the final kinetic energy is lower than the initial one,

$$\begin{aligned}&\frac{1}{2}m_A\left(v_{A_1}^2 + k_A^2\omega_{A_1}^2\right) + \frac{1}{2}m_B\left(v_{B_1}^2 + k_B^2\omega_{B_1}^2\right)\\ &> \frac{1}{2}m_A\left(v_{A_2}^2 + k_A^2\omega_{A_2}^2\right) + \frac{1}{2}m_B\left(v_{B_2}^2 + k_B^2\omega_{B_2}^2\right),\end{aligned} \tag{A2}$$

where $k_A^2\omega_{A1}^2$ and $k_B^2\omega_{B1}^2$ account for the contribution of the rotations of the two bodies in the kinetic energy. Generally we are interested in obtaining a relationship between the running conditions before impact (velocities at instant t_1) and those after impact (velocities at instant t_2). The contact surface between the two vehicles at the instant when maximum deformation occurs is assumed to be plane; the resultant of contact forces is applied in O where the reference system Oxy is centred. The x-axis is perpendicular to the contact surface. The impact duration is considered to be vanishing, so the two vehicle bodies can be thought to be pre-deformed as shown in Figure A1.

The point O can be considered as belonging to vehicle A or to vehicle B; the vehicle velocities are, respectively,

$$\vec{V}_{A_O} = \begin{cases} v_A + \omega_A y_A \\ u_A - \omega_A x_A \end{cases} \quad \vec{V}_{B_O} = \begin{cases} v_B - \omega_B y_B \\ u_B + \omega_B x_B \end{cases}. \tag{A3}$$

The relative velocity of vehicle B with respect to vehicle A is

$$\vec{V}_r = \begin{cases} v_A + v_B + \omega_A y_A - \omega_B y_B \\ u_A + u_B - \omega_A x_A + \omega_B x_B \end{cases}. \tag{A4}$$

Considering the coefficient of restitution e, the relative velocities before and after impact can be related,

$$\vec{V}_{r_2} = -e\vec{V}_{r_1}. \tag{A5}$$

From the impulse theorem, we have

$$\begin{aligned}\vec{I} &= \int_{t_1}^{t_2} \vec{F}\, dt = \langle\vec{F}\rangle(t_2 - t_1)\\ &= m_A\vec{v}_{A_2} - m_A\vec{v}_{A_1} = m_B\vec{v}_{B_2} - m_B\vec{v}_{B_2}.\end{aligned} \tag{A6}$$

The impulse theorem can be written in scalar form as

$$\begin{cases} I_x = m_B(v_{B_2} - v_{B_1}) \\ I_y = m_B(u_{B_2} - u_{B_1}) \end{cases} \quad \begin{cases} -I_x = m_A(v_{A_2} - v_{A_1}) \\ -I_y = m_A(u_{A_2} - u_{A_1}) \end{cases}. \tag{A7}$$

We can write

$$I_y = \lambda I_x, \tag{A8}$$

where λ is a parameter accounting for friction and interlocking between the two contact surfaces. So the

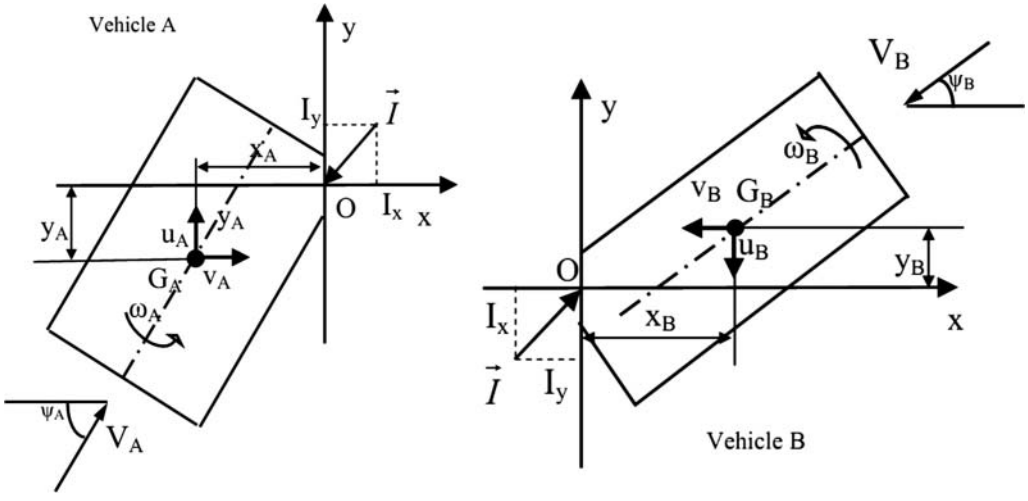

Figure A1. Forces acting at the contact surface between vehicles A and B.

equations of the conservation of motion can be written as

$$\begin{cases} m_A v_{A_1} - I_x = m_A v_{A_2} \\ m_A u_{A_1} - \lambda I_x = m_A u_{A_2} \\ m_A k_A^2 \omega_{A_1} - I_x y_A + \lambda I_x x_A = m_A k_A^2 \omega_{A_2} \end{cases} \quad \text{(A9)}$$

$$\begin{cases} m_B v_{B_1} - I_x = m_B v_{B_2} \\ m_B u_{B_1} - \lambda I_x = m_B u_{B_2} \\ m_B k_B^2 \omega_{B_1} + I_x y_B - \lambda I_x x_B = m_B k_B^2 \omega_{B_2} \end{cases}.$$

From a guess value of the velocities before the impact and considering Equations (A4), (A5) and (A9), the relative velocity after the impact can be computed as

$$\begin{aligned} v_{r_2} &= v_{r_1} - I_x(A - \lambda B) = -e v_{r_1} \\ A &= \frac{1}{m_A} + \frac{1}{m_B} + \frac{y_A^2}{m_A k_A^2} + \frac{y_A^2}{m_B k_B^2} \\ B &= \frac{x_A y_A}{m_A k_A^2} + \frac{x_B y_B}{m_B k_B^2}. \end{aligned} \quad \text{(A10)}$$

Then, the impulse of the force can be estimated as

$$I_x = \frac{1+e}{A - \lambda B} v_{r_1}. \quad \text{(A11)}$$

And, finally, the velocities after the impact are

$$\begin{cases} v_{A_2} = v_{A_1} - I_x / m_A \\ u_{A_2} = u_{A_1} - \lambda I_x / m_A \\ \omega_{A_2} = \omega_{A_1} - I_x (y_A - \lambda x_A)/(m_A k_A^2) \end{cases} \quad \text{(A12)}$$

$$\begin{cases} v_{B_2} = v_{B_1} - I_x / m_B \\ u_{B_2} = u_{B_1} - \lambda I_x / m_B \\ \omega_{B_2} = \omega_{B_1} + I_x (y_B - \lambda x_B)/(m_B k_B^2) \end{cases}. \quad \text{(A13)}$$

A direct application of these formulae is difficult due to the presence of λ and e, whose values are not easy to be evaluated. It is also necessary to know the position and the direction of x- and y-axes exactly. The reference system origin O is defined as the point where the resultant of the exchanged forces between vehicles is applied.

Appendix 2. JARI 1 parameter list

JARI 1	Vehicle A	Vehicle B
Mass (kg)	981	974
Wheelbase (m)	2.5	2.5
Track (m)	1.35	1.35
CG location (from front axle) (m)	1.03	1.03
Yaw moment of inertia (kg m^2)	1485	1475
Friction coefficient (–)	0.8–0.9	0.8–0.9
Rolling resistance (–)	0.01	0.01
Steer angle *dx*/*sx* (°)	0/0	0/0
Maximum slip angle (°)	10	10
Initial CG *x* coordinate (m) (see Figure A1)	−1.05	1.28
Initial CG *y* coordinate (m) (see Figure A1)	−0.84	0.07
Initial angle between longitudinal vehicle axis and *x* axis (°) (see Figure A1)	47	182
Blocked wheels	Both front	Both front
Final CG *x* coordinate (m) (see Figure A1)	−1.53	0.7
Final CG *y* coordinate (m) (see Figure A1)	2.73	0.32
Final angle between longitudinal vehicle axis and *x* axis (°) (see Figure A1)	63	62
Coefficient of restitution (–)	0.15	
Coefficient of interlocking, friction (–)	0.35–0.45	
Acceptable error threshold $E_{t\text{adm}}$ (m)	1	
Acceptable error threshold $E_{\theta\text{adm}}$ (°)	17	

Appendix 3. JARI 4 parameter list

JARI 4	Vehicle A	Vehicle B
Mass (kg)	1737	1728
CG location (from front axle) (m)	1.10	1.10
Yaw moment of inertia (kg m^2)	3325	3307
Wheelbase (m)	2.84	2.84
Track (m)	1.55	1.55
Friction coefficient (–)	0.7–0.9	0.6–0.8
Rolling resistance (–)	0.01	0.01
Steer angle *dx*/*sx* (°)	0/0	0/0
Maximum slip angle (°)	10	10
Initial CG *x* coordinate (m) (see Figure A1)	−0.74	1.36
Initial CG *y* coordinate (m) (see Figure A1)	−0.97	−0.69
Initial angle between longitudinal vehicle axis and *x* axis (°) (see Figure A1)	269,5	149.5
Blocked wheels	Both front	Both front
Final CG *x* coordinate (m) (see Figure A1)	3.49	10.51
Final CG *y* coordinate (m) (see Figure A1)	14.74	14.98
Final angle between longitudinal vehicle axis and *x* axis (°) (see Figure A1)	65	−141
Coefficient of restitution (–)	0.2	
Coefficient of interlocking, friction (–)	0.8–1.8	
Acceptable error threshold $E_{t\text{adm}}$ (m)	1	
Acceptable error threshold $E_{\theta\text{adm}}$ (°)	17	

Appendix 4. JARI 5 parameter list

JARI 5	Vehicle A	Vehicle B
Mass (kg)	977	976
CG location (from front axle) (m)	0.99	1.00
Yaw moment of inertia (kg m^2)	1460	1464
Wheelbase (m)	2.5	2.5
Track (m)	1.35	1.35
Friction coefficient (–)	0.7–1	0.7–1
Rolling resistance (–)	0.01	0.01
Steer angle *dx*/*sx* (°)	0/0	0/0
Maximum slip angle (°)	10	10
Initial CG *x* coordinate (m) (see Figure A1)	1.713	0.322
Initial CG *y* coordinate (m) (see Figure A1)	0.730	1.586
Initial angle between longitudinal vehicle axis and *x* axis (°) (see Figure A1)	24	269
Blocked wheels	Left front	Both rear
Final CG *x* coordinate (m) (see Figure A1)	−6.22	22.83
Final CG *y* coordinate (m) (see Figure A1)	20.3	7.35
Final angle between longitudinal vehicle axis and *x* axis (°) (see Figure A1)	−74	101
Coefficient of restitution (–)	0.05–0.1	
Coefficient of interlocking, friction (–)	0.6–0.9	
Acceptable error threshold E_{radm} (m)	1	
Acceptable error threshold $E_{\theta adm}$ (°)	17	

(*continued*)